Impact of Alkali Metal Cations and Iron Impurities on the Evolution of Hydrogen on Cu Electrodes in Alkaline Electrolytes

Journal of The Electrochemical Society, 2020 **167** 106505
1945-7111/2020/167(10)/106505/7/$40.00 © 2020 The Electrochemical Society ("ECS"). Published on behalf of ECS by IOP Publishing Limited

Impact of Alkali Metal Cations and Iron Impurities on the Evolution of Hydrogen on Cu Electrodes in Alkaline Electrolytes

Xiang Li,[1] Charuni M. Gunathunge,[1] Naveen Agrawal,[2,*] Hansel Montalvo-Castro,[2] Jing Jin,[1] Michael J. Janik,[2,z] and Matthias M. Waegele[1,z]

[1]*Department of Chemistry, Merkert Chemistry Center, Boston College, Chestnut Hill, Massachusetts 02467, United States of America*
[2]*Department of Chemical Engineering, 121 Chemical and Biomedical Engineering Building, The Pennsylvania State University, University Park, Pennsylvania 16802, United States of America*

Electrocatalytic Cu is key to the development of processes that can convert CO and CO_2 to hydrocarbons, and nitrate to ammonia. The hydrogen evolution reaction (HER) often competes with these processes. Few studies studied this reaction on Cu under alkaline conditions. Herein, we examined the HER on Cu electrodes under alkaline conditions in Na^+- and Cs^+-containing electrolytes. We found that in 0.1 M solutions of NaOH and CsOH of the highest commercially available purity grades, trace impurities of iron deposit on the Cu electrode during electrolysis. As a result, the rate of the HER is enhanced by up to a factor of ≈5 over the course of eleven cyclic voltammograms (CV) from 0.15 to −0.65 V vs the reversible hydrogen electrode. After removal of the iron impurities, the CVs are stable as a function of cycle number. Comparison of the CVs in pre-electrolyzed 0.1 M NaOH and CsOH reveals that changing the cation from Na^+ to Cs^+ has no measurable effect on the HER. With density functional theory (DFT), we further rationalized our experimental findings. We discuss the implications of our results for electrocatalytic processes on Cu electrodes.
 [DOI: 10.1149/1945-7111/ab987b]

Manuscript submitted April 8, 2020; revised manuscript received May 27, 2020. Published June 11, 2020.

Supplementary material for this article is available online

The hydrogen evolution reaction (HER) is a common side reaction of many technologically relevant electroreduction processes in aqueous solutions. For example, during the electroreduction of CO_2 to hydrocarbons on polycrystalline Cu electrodes in pH-neutral electrolyte, the Faradaic efficiency for hydrogen is ≈30% at an applied potential of −0.9 V vs the reversible hydrogen electrode (RHE).[1] Understanding the HER on Cu electrodes is of particular technological interest. Cu is the only pure metal that can reduce CO_2 to hydrocarbons at appreciable rates[2–4] and it is the most active coinage metal for the reduction of nitrate to ammonia.[5] In both processes, the HER on Cu is a major side reaction. To improve the selectivity for desirable products, strategies for suppressing the HER while promoting the desired reactions need to be developed. Tuning the composition of the electrolyte is a promising strategy for altering the relative rates of the competing interfacial reactions.[6–9] To effectively deploy this strategy, it is essential to understand how the HER on Cu is affected by the composition of the electrolyte.

Despite the central role of the HER as a competing reaction in the reductions of CO_2, CO, and nitrate on Cu electrodes, investigations of the HER on Cu in alkaline electrolytes are rare.[10–13]Understanding the HER under alkaline conditions is particularly important because electrolyzers for CO_2 or CO reduction are typically operated at high pH,[15–17] where the overpotentials for the formation of desirable products such as ethylene are lowered by up to several hundreds of millivolts relative to those at neutral pH.[18]

Apart from carrying out the electrolysis under alkaline conditions, desirable reactions can be promoted by judicious choice of the cation of the supporting electrolyte.[19] For example, the rate of the reduction of surface-adsorbed CO on Cu electrodes is enhanced by about one order of magnitude upon switching from Li^+- to Cs^+-containing electrolyte.[20] In another study on the reduction of CO on Cu, ethylene formation was observed in the presence of $methyl_4N^+$, whereas no appreciable formation of this product was found in the presence of $butyl_4N^+$.[21]

The effects of cations on electrocatalytic processes were first discovered in the context of the HER on mercury electrodes.[22] In a more recent study, an enhancement of the HER on $Ir_{0.5}Ru_{0.5}$ electrodes in 0.1 M KOH by nearly a factor of two was reported upon addition of Li^+ (10^{-2} M) or Ba^{2+} (10^{-4} M).[23] Similarly, the modulation of the rates of the HER on Pt, Ir, Ag, and Au electrodes by up to a factor of ≈4 was observed upon switching the electrolyte from 0.1 M CsOH to LiOH.[24] Increasing the ionic strength was also shown to promote the HER on Pt/Ni electrodes.[25] However, the impact of alkali metal cations on the HER on Cu electrodes has only been parenthetically discussed in the recent CO_2/CO reduction literature. For example, in a recent study on the electroreduction of CO_2 on Cu electrodes at neutral pH, the partial current density of the HER was found to be virtually independent of the identity of the alkali metal cation in solution.[9] By contrast, at pH 13, an increased HER activity was reported with increasing size of the alkali metal cation in a study on the reduction of CO on Cu.[26] In these two studies, CO_2 or CO reduction occurred concurrently to the HER. A systematic study of the effects of alkali metal cations on the HER on Cu electrodes under alkaline conditions and in the absence of other Faradaic reactions is missing to date.

In comparison to other earth-abundant metals, such as Fe, Ni, Co, and W, Cu is a relatively poor HER catalyst.[12] For example, the polarization curve for the HER on iron is shifted by ≈250 mV in the anodic direction relative to that for the reaction on Cu. Traces of metal impurities are well known to give rise to apparent electrocatalytic activity.[27–30] For example, trace amounts of Cu on carbon-based electrodes are responsible for their apparent CO_2 reduction activity.[29] Similarly, metal impurities in heteroatom-doped graphene electrodes give rise to the oxygen reduction activity of these electrodes.[27] Impurities in the electrolyte can also deposit on the electrode during electrolysis. For example, iron traces in alkali metal hydroxide electrolytes enhance the rate of the water oxidation reaction on nickel-iron oxyhydroxides.[28,30] Alkali metal hydroxides typically contain more trace metal impurities compared to other commercially available high-purity salts. It is therefore essential to ascertain to what extent such impurities impact the HER on Cu.

In this work, we studied the HER on a polycrystalline Cu rotating disk electrode (RDE) in Na^+ and Cs^+-containing electrolytes under alkaline conditions. We found that trace amounts of iron impurities in hydroxide salts of the highest commercially available purity grades substantially increase the rate of the HER at a pH of 13. Specifically, in 0.1 M CsOH, the HER current density increased by a

*Electrochemical Society Student Member.
[z]E-mail: mjanik@psu.edu; waegele@bc.edu

factor of five over the course of eleven cyclic voltammograms (CV) due to the deposition of iron on the Cu RDE. Without iron impurities, the HER currents in 0.1 M NaOH and CsOH electrolytes are virtually the same, indicating the absence of a measurable cation effect on the HER. With density functional theory (DFT), we found that the hydrogen binding energy to Cu(100) is only slightly perturbed in the presence of co-adsorbed alkali metal cations. Further, the cations would need to induce large changes of about $\geqslant 0.3$ V Å^{-1} in the local electric field to impact the activation barrier of the Volmer step of the HER. Because Cs^+ is known to promote CO_2/CO reduction on Cu electrodes,[9,20,26,31] our observations suggest that Cs^+ can be utilized to selectively enhance this desired reaction over the HER. Optimal catalytic performance in alkali metal hydroxides can only be achieved by efficient removal of iron impurities prior to electrolysis.

Experimental

Materials.—Sodium hydroxide (99.99%) was obtained from MilliporeSigma. Cesium hydroxide monohydrate (99.95%; Acros Organics), nitric acid (TraceMetal grade, 67%–70%; Fisher) and boric acid (Puratronic 99.9995%; Alfa Aesar) were acquired from Fisher Scientific. Ar (ultra high purity) was obtained from Air Gas (Radnor, PA).

Electrode preparation.—The custom-built RDE consisted of a Cu rod (5 mm diameter, 99.999%, Fisher Scientific; Waltham, MA) that was installed in a polyether ether ketone (PEEK) holder. The RDE was polished to a mirror finish with 1 μm diamond paste (Ted Pella; Redding, CA) for 10 min and 0.3 μm alumina slurry (Electron Microscopy Sciences; Hartfield, PA) for 3 min. Then, the RDE was sonicated in high-purity water for 10 min and dried under a stream of ultra high-purity N_2. The RDE was then electropolished in a mixture of H_3PO_4 (85 wt%) : H_2O : H_2SO_4 (95 wt%) (volume ratio of 10:5:2).[32] The electropolishing protocol consisted of two independent segments of chronopotentiometry for 2 s at a current density of 100 μA cm^{-2} and a 30 s interval at open circuit potential in between them. Then, the RDE was thoroughly rinsed with high-purity water and installed in the electrochemical cell.

Electrochemical measurements.—Electrochemical measurements were carried out in a two-compartment As-free glass cell separated by a Selemion AHO ion exchange membrane (AGC Engineering Co.; Chiba, Japan). 65 ml and 15 ml of electrolyte were used for the working and counter electrode compartments, respectively. 0.1 M NaOH or CsOH electrolyte was freshly prepared right before each experiment from the corresponding 1 M stock solution that was stored in a plastic bottle. The pH of the bulk electrolyte was ≈12.8 for 0.1 M NaOH and ≈12.9 for 0.1 M CsOH. The electrolyte of pH 9 was prepared by titrating the corresponding alkali hydroxide solution with boric acid. The final concentration of alkali cations was 0.1 M. Data collection was typically completed within one hour.

The electrolyte was purged with ultra high-purity Ar at a flow rate of 30 standard cubic centimeters per minute (sccm) in the working electrode compartment and 10 sccm in the counter electrode compartment for 15 min before the start of the measurement. Purging was continued until completion of the experiment. An Au wire (Premion 99.999%, 0.5 mm diameter; Alfa Aesar) was used as the counter electrode and an Hg/HgO electrode (EF1369, 1 M NaOH; BASi Inc.; West Lafayette, IN) was used as the reference electrode. The potential of the Hg/HgO reference electrode was routinely checked against a saturated calomel electrode to ensure electrode stability. A VSP electrochemical workstation (Biologic; Knoxville, TN) was used to control the potential. The surface roughness of the electrode was determined by electrochemical capacitance measurements.[33]

Eleven consecutive CVs with turning potentials of 0.15 and ≈−0.65 V vs RHE at a scan rate of 10 mV s^{-1} were carried out in 0.1 M NaOH and CsOH. For Na^+ and Cs^+-containing electrolytes at a pH of 9, CVs from 0.0 to ≈−0.9 V vs RHE were carried out. The 2nd, 6th, and 11th cycles were used for Tafel analysis. The real cathodic turning potentials slightly varied for consecutive CVs because 15% of the *iR*-drop was manually corrected following the measurements. Following the CVs, steady-state measurements were carried out. Five potential steps were selected. At each potential step, the potential was held for 3 min and the average of the last minute was used for analysis.

The applied potential vs the Hg/HgO electrode was converted to the RHE scale by application of the equation: $E_{RHE} = E_{Hg/HgO} + 0.147\ V + pH \times 0.059\ V$. The solution resistance between reference and working electrodes was ≈40 Ohms for 0.1 M alkali metal hydroxide electrolytes and ≈110 Ohms for pH 9 electrolytes. 85% of the *iR*-drop was compensated by the potentiostat during the experiment. The remaining 15% of the *iR*-drop was manually corrected after completion of the experiment according to: $E_{real} = E_{measured} - iR_u$, where R_u is the uncompensated resistance. All reported current densities are based on the geometric area of the RDE.

Pre-electrolysis.—80 ml of 0.1 M NaOH or CsOH electrolyte was prepared from the corresponding 1 M stock solution. Two pieces of Cu foil (Puratronic 99.999%, 0.025 mm; Alfa Aesar) were used as working and counter electrodes. The surface area of the working electrode was 12.5 cm^2. The electrolysis was carried out in a polypropene bottle under stirring of the electrolyte at 200 rpm and under purging of the electrolyte with Ar at 10 sccm. The applied potential was −2 V vs a Cu rod. The electrodes were removed from the electrolyte under applied bias after ≈20 hours. Deep red precipitate (Cu oxides from oxidation of the Cu anode) was removed by filtration of the electrolyte with a 0.22 μm polytetrafluoroethylene syringe filter (Fisherbrand).

X-ray photoelectron spectroscopy (XPS).—The X-ray photoelectron spectra were collected on a Surface Science S-Probe ESCA with an Al Kα X-ray source. Narrow scans over peaks of interest were collected with a step size of 0.065 eV. The operating pressure was ≈10^{-7} torr. The X-ray spot was 300 μm in diameter. The X-ray source was operated at 5 mA and 10 kV.

Inductively coupled plasma—atomic emission spectroscopy (ICP-AES).—Samples were prepared by adding 86 μl of 70% HNO_3 to 3 ml of the 0.1 M alkali metal hydroxide solution. The samples were analyzed on an Agilent 5100 ICP-AES instrument. Calibration curves for Ni and Fe were derived from standard solutions (25, 50, 100, 250, 500, 1000 nM) of the corresponding salts.

Results and Discussion

Effect of trace iron and nickel impurities on the HER on Cu electrodes.—We first measured the rates of the HER on a polycrystalline Cu RDE in 0.1 M aqueous solutions of NaOH and CsOH during eleven consecutive CVs with turning potentials of 0.15 and ≈−0.65 V vs RHE. All potentials were corrected for the *iR*-drop and were referenced against RHE, unless otherwise noted. The real cathodic turning potentials slightly varied for consecutive CVs because 15% of the *iR*-drop was corrected post run. The scan rate of the electrode potential was 10 mV s^{-1} and the rotation rate of the RDE was 2500 rpm. For this set of measurements, the electrolytes were prepared by dissolving the as-received hydroxide salts in high-purity water. The purities of NaOH and CsOH were 99.99% and 99.95%, respectively. Further details are provided in the experimental procedures section.

Figure 1 shows representative CVs of Cu in the two electrolytes. For clarity, the most anodic potential in the graphs is −0.2 V, but the anodic turning potentials of the CVs was +0.15 V. The current density increases with increasing cycle number in both electrolytes.

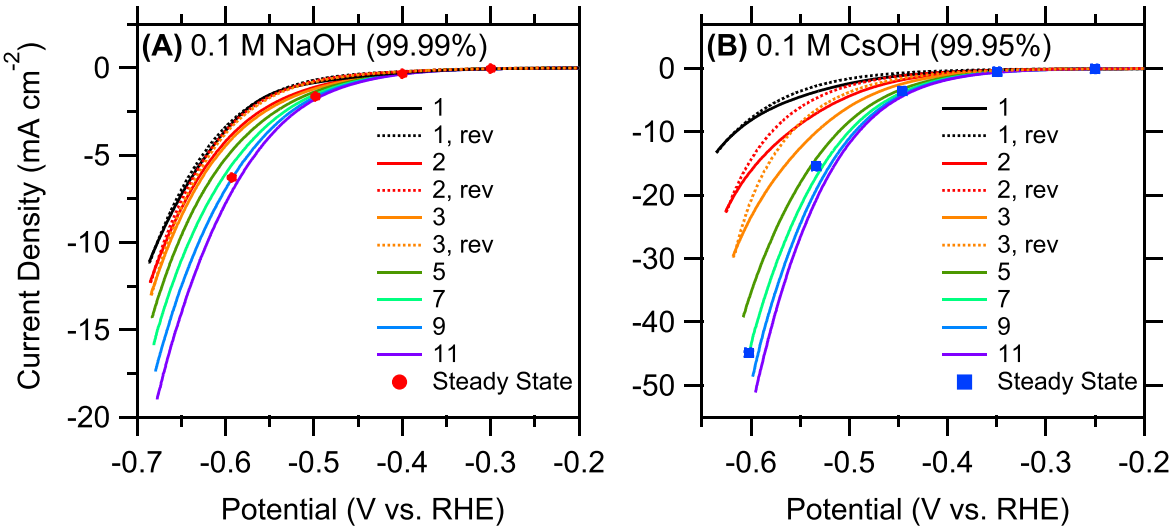

Figure 1. Consecutive CVs of a polycrystalline Cu RDE in 0.1 M solutions of as-received (A) NaOH (99.99%) and (B) CsOH (99.95%). The CVs were taken at a scan rate of 10 mV s^{-1} and a rotation rate of 2500 rpm of the RDE. The purity of each salt is indicated in the parenthesis in each panel. The numbers in the panels refer to the cycle number and "rev" denotes the respective reverse (anodic) scan. For clarity, the reverse scans of the other cycles are not shown. Steady-state measurements were collected right after the eleventh CV.

However, whereas the current density approximately doubles in 0.1 M NaOH over the course of the eleven CVs, it increases by about a factor of five in 0.1 M CsOH. The steady-state current densities, which were taken right after completion of the eleven CVs, closely coincide with the final CVs. These data indicate that the electrode undergoes more substantial, irreversible changes in 0.1 M CsOH than in 0.1 M NaOH.

The increase in the HER rate could arise from a number of different reasons, including cationic corrosion,[34] oxidation/reduction-induced surface reconstruction,[35] adsorbate-induced reconstruction,[36] or deposition of trace elements from the electrolyte on the electrode.[28]

Cationic corrosion is expected to require significantly more cathodic potentials (−1.0 V vs RHE) and higher electrolyte concentrations (⩾1 M) compared to those employed here.[34] Electrolyte-induced surface reconstructions can also occur during oxidation/reduction cycles.[35] However, during our CVs, the electrodes were never exposed to oxidizing conditions. Moreover, cationic corrosion and electrolyte-induced restructuring typically result in substantially roughened surfaces. However, in the present case, the electric double layer capacitance increased by only ≈10% over the course of the CVs, suggesting that the roughness of the electrode did not significantly change. On the basis of prior work, we expect that residual surface oxides and hydroxides will be almost completely removed after the first CV.[33] For these reasons, we exclude these two processes as the underlying reason for the increase in HER activity.

While reconstructions on the nano- and micro-scales apparently do not occur to any significant extent under our reaction conditions, changes of the predominant surface adsorbates with potential may affect the surface at the atomic level. Surface-reconstructions due to the adsorption of hydrogen have been reported for Cu(100) electrodes at pH values <3, but no such changes in the surface were found at higher pH values.[36] At pH 13, the (100) facet is remarkably stable and the major surface facet on polycrystalline Cu.[37] Therefore, it is unlikely that atomic-level reconstructions are the origin of the changes in catalytic activity.

Lastly, the change in catalytic activity could arise from the deposition of trace metal impurities, as was reported for other electrocatalytic processes.[28,30] Although the used hydroxides are of the highest purity grades that are commercially available, they contain trace amounts of nickel and iron. Table I shows that both alkali metal hydroxides contain a significant amount of iron and/or nickel. No detectable amount of nickel was found in CsOH. The values in Table I are based on the analyses provided by the manufacturers of the salts. We obtained virtually the same values from the analyses of the electrolytes by ICP-AES. The full elemental analyses from the manufacturers are provided in Table SI (Supplementary Material is available online at stacks.iop.org/JES/167/106505/mmedia). Other major impurities are alkali and earth alkaline ions, which cannot be reduced on the Cu electrode under our experimental conditions. Iron species are the only trace metal impurities that occur at detectable levels in both electrolytes and are expected to be readily reduced at the most cathodic potentials accessed in this study. Nickel and iron are substantially better electrocatalysts for the HER than Cu: Their polarization curves are shifted by ≈250 mV more anodically relative to the HER polarization curve for Cu.[12] Therefore, deposition of either of the species on the Cu electrode is expected to enhance the rate of the HER.

To test if iron and nickel deposit on the Cu RDE during electrolysis, we examined the electrode with XPS following 1.9 h of electrolysis at a potential of −0.68 V for 0.1 M NaOH and −0.60 V for 0.1 M CsOH. The RDE was removed from the electrolyte under applied bias to minimize dissolution of the deposit into the electrolyte. The electrochemical currents as a function of time are provided in Fig. S1.

As shown in Fig. 2, following electrolysis in 0.1 M CsOH (99.95%), the RDE exhibits the characteristic peaks of iron. Iron deposits after electrolysis in 0.1 M NaOH (99.99%) were below the detection limit of the XPS instrument. Interestingly, even though this electrolyte contains a significant amount of nickel (Table I), nickel deposits were below the detection limit.

The amount of iron that deposits during the measurement depends on the diffusion flux of iron species to the RDE, $J = Dc_b/\delta$,[38] where D, c_b, and δ are the diffusion coefficient, the bulk concentration of iron, and the diffusion layer thickness, respectively. Assuming $D = 1 \times 10^{-5}$ cm^2 s^{-1}, $c_b = 240$ nM, and $\delta = 10$ μm, and that a monolayer is approximately equal to 2 nmol cm^{-2}, we find that a complete monolayer forms within ≈15 min. For this rough estimate, we assumed that every reducible ion that arrives at the electrode deposits on it. Although the electrode potential may not be sufficiently negative at all times to reduce iron impurities during the CV measurements, this result is a useful order-of-magnitude estimate. Because electrocatalytic processes can be affected by coverages well below a monolayer, this order-of-

Table I. Nanomolar (nM) concentrations of iron and nickel in 0.1 M solutions of the as-received alkali metal hydroxides.

Electrolyte	Fe (nM)	Ni (nM)
0.1 M NaOH (99.99%)	40	180
0.1 M CsOH (99.95%)	240	/

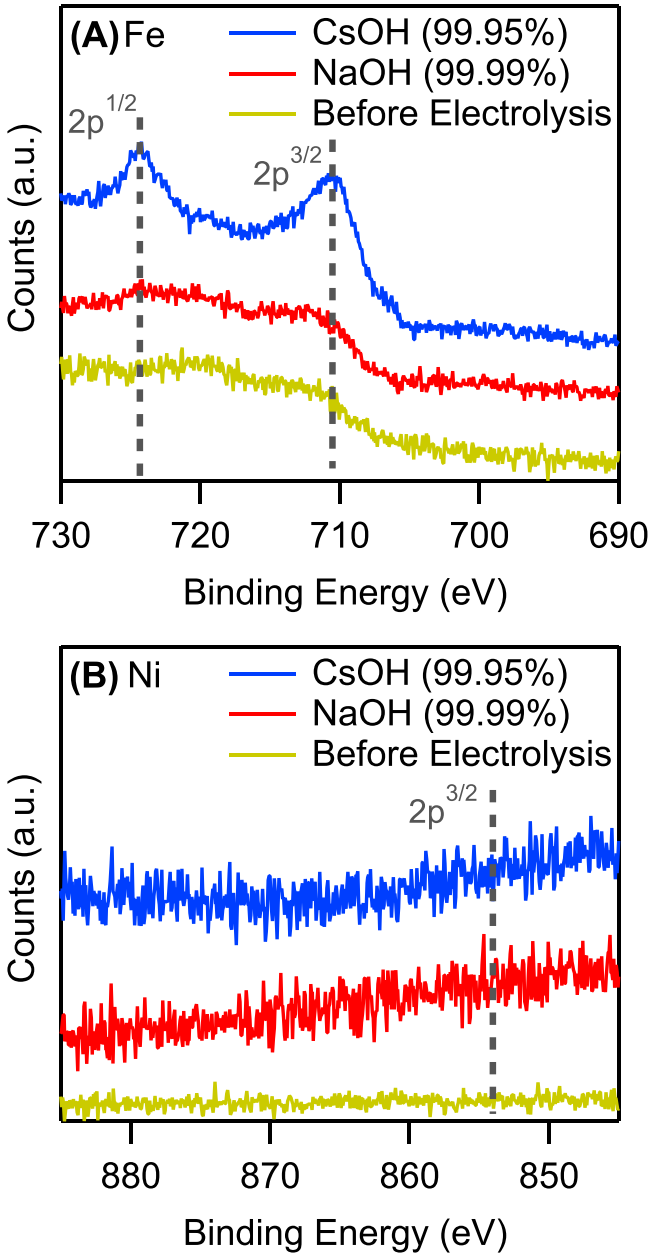

Figure 2. X-ray photoelectron spectra of the Cu RDE before and after 1.9 h of electrolysis in the regions for (A) Fe and (B) Ni.

magnitude estimate shows that significant amounts of iron can deposit over the course of the CV experiments.

In summary, 0.1 M CsOH (99.95%) contains about six times more iron than 0.1 M NaOH (99.99%) (Table I). A larger enhancement of the HER over the course of eleven CVs occurs in the former electrolyte (Fig. 1). XPS confirms the presence of iron on the Cu RDE following prolonged electrolysis in 0.1 M CsOH (99.95%). Taken together, these findings show that the deposition of iron impurities is likely the origin of the HER activity changes during the CVs. It is probable that nickel also contributes to the enhancement, but this impurity apparently does not deposit as efficiently on the Cu RDE.

Impact of iron deposits on Tafel slopes and exchange currents.—To understand better how the trace iron impurities affect the HER on the Cu electrode, we conducted Tafel analyses of the current densities. Following established procedures,[39] we restricted the analysis of the Tafel slope to overpotentials significantly larger than 1/2 of the absolute value of the Tafel slope (0.2 V), and to sufficiently small current densities at which no apparent mass transport limitations are expected (<10 mA cm^{-2}). Comparison of data collected at 1500 and 2500 rpm indicates the absence of transport limitations (Fig. S2).

Figure 3 shows the 10-based logarithm of the current density as a function of overpotential during the cathodic forward scan of the second CV for each electrolyte. Additional representative data for the 6th and 11th CVs are shown in Fig. S3. As shown in Table II, the Tafel slope decreases with increasing cycle number in both electrolytes. Irrespective of the cycle number, the Tafel slope for the HER in CsOH (99.95%) is consistently smaller by 35 ± 5 mV dec^{-1} compared to that for the reaction in NaOH (99.99%). Interestingly, the exchange current densities slightly decrease by a factor of 2–3 over the course of the eleven CVs. Although this decrease may be an artifact of the extrapolation, it unequivocally shows that the promotion of the HER with cycle number is due to a decrease in the Tafel slope as iron deposits on the Cu electrode.

The Tafel slope is a function of the symmetry factor of the rate-determining step (RDS) of the reaction and the coverage of surface-adsorbed species.[40] It is possible that the deposition of iron switches the RDS to a different elementary step in the reaction mechanism or alters the value of the symmetry factor for the same RDS. However, the deposition of iron on the Cu electrode is also expected to significantly change the surface coverage of hydrogen. The absolute value of the binding energy of hydrogen to iron is about 0.4 eV larger than the corresponding value for Cu.[12] If it is assumed that the RDS of the reaction is the Volmer step and that the reaction proceeds via the Volmer-Heyrovsky pathway, it is straightforward to show that the apparent transfer coefficient is $\alpha = \beta + \theta_H$, where β is the symmetry factor of the Volmer step and θ_H is the surface coverage of hydrogen. The Tafel slope is inversely proportional to the apparent transfer coefficient.[40] Therefore, the observed decrease in the Tafel slope with cycle number is consistent with an increase of the surface-coverage of hydrogen upon deposition of iron on the Cu electrode.

Impact of iron on the HER at pH 9.—To test if the enhancement of the HER by iron impurities also occurs at a lower pH, we prepared 0.1 M solutions of Na^+ and Cs^+ at a pH of 9 from the as-received alkali metal hydroxide salts. The pH of the solutions was adjusted with boric acid. In contrast to the observations at pH 13, the CVs were relatively stable with cycle number (Fig. S4). The Tafel slopes of the HER in Na^+- and Cs^+-containing electrolytes at a pH of 9 are essentially identical (Fig. S5). However, in comparison to the CVs, the steady-state current density in the electrolyte prepared from CsOH (99.95%) is significantly shifted toward more anodic potentials (Fig. S4). This observation suggests that the deposition of iron on the Cu RDE is slower at pH 9 than at pH 13. The slower kinetics of iron deposition could arise from a number of factors, including the presence of different predominant iron species in solution or pH-dependent electric double layer properties that render the deposition of iron on the electrode kinetically less favorable. These results show that for a given concentration of iron impurities, the rate enhancement of the HER increases with increasing pH.

Effects of cations on the HER.—To test if the HER is promoted by Cs^+ relative to the reaction in Na^+-containing electrolyte, we purified the alkali metal hydroxide solutions by pre-electrolysis. Details of the pre-electrolysis protocol are provided in the

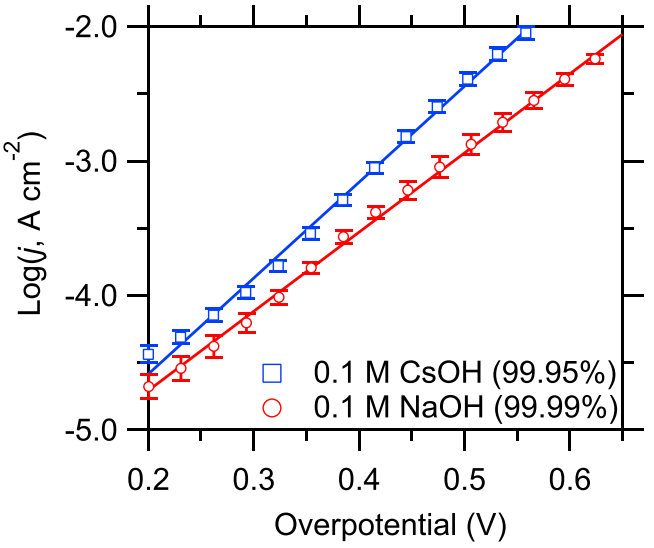

Figure 3. Tafel plots for the forward (cathodic) scans of the second CVs. The data represent the average of six independent experiments for each electrolyte. The error bars represent one standard deviation. For clarity, only a subset of the collected data points is shown on the plot. The Tafel plots for the 6th and 11th cycles are reported in Fig. S3.

the concentration of iron in the pre-electrolyzed electrolytes was typically <25 nM.

Comparison of the current densities in Figs. 4A and 4B reveals that the HER proceeds at nearly the same rates in Na^+- and Cs^+-containing electrolytes. Indeed, the Tafel plots for the HER current densities in the two electrolytes mostly overlap (Fig. 5). The extracted Tafel slopes (163 ± 3 mV dec^{-1} in NaOH and 173 ± 13 mV dec^{-1} in CsOH) and exchange current densities ($\log[j_0, A\ cm^{-2}] = -6.05 \pm 0.09$ in NaOH and -5.83 ± 0.17 in CsOH) for the two different electrolytes are statistically not significantly different, indicating the absence of a detectable cation effect.

The observation that the switch from Na^+- to Cs^+-containing electrolyte has no measurable effect on the rate of the HER is surprising for the following reasons: First, the rates of other small-molecule electrocatalytic reactions are strongly affected when switching the cation of the supporting electrolyte from Na^+ to Cs^+.[19] For example, the rate of ethylene formation during the reduction of CO_2 is enhanced by a factor of ≈6 in the presence of Cs^+ relative to that in Na^+-containing electrolyte.[9] Cs^+ also shifts the half-wave potential of the oxygen evolution reaction on Pt by ≈50 mV in the cathodic direction relative to that in the presence of Na^+.[41] These examples demonstrate that the two cations have the potential to structure the electric double layer in distinct ways that result in different electrocatalytic properties of the interface. Second,

Table II. Tafel slopes and exchange current densities for the HER on Cu. The standard deviations are based on six independent measurements for each 0.1 M electrolyte prepared from the as-received hydroxide salts (NaOH (99.99%) and CsOH (99.95%)). The reported data were derived from the forward scan of the CVs.

	Tafel Slopes (mV dec^{-1})		log (j_0, A cm^{-2})	
Cycle	NaOH	CsOH	NaOH	CsOH
2	170 ± 7	140 ± 6	−5.88 ± 0.12	−6.01 ± 0.11
6	157 ± 5	117 ± 2	−6.12 ± 0.23	−6.33 ± 0.08
11	149 ± 5	111 ± 1	−6.12 ± 0.12	−6.46 ± 0.08

experimental procedures section. Figure 4 shows that the CVs of the polycrystalline Cu electrodes do not significantly change as a function of cycle number in the pre-electrolyzed electrolytes. This observation suggests that the pre-electrolysis procedure successfully removed trace impurities of iron. With ICP-AES, we confirmed that

water has a large electric dipole moment (1.9 Debye).[42] DFT models show that Cs^+ retains more charge upon its specific adsorption on metal surfaces compared to Na^+.[43] Therefore, the water dissociation steps (Volmer and Heyrovsky reactions), which may involve water in the hydration shells of cations, are expected to be differently impacted by Cs^+ and Na^+. Third, the concentration of hydronium

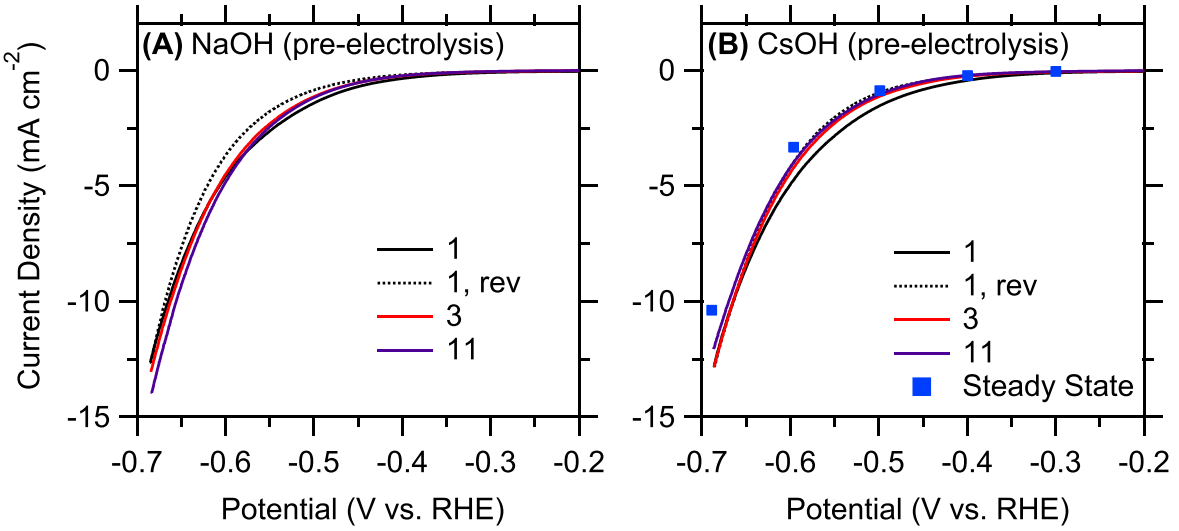

Figure 4. Consecutive CVs of a polycrystalline Cu RDE in 0.1 M solutions of pre-electrolyzed (A) NaOH and (B) CsOH. The CVs were taken at a scan rate of 10 mV s^{-1} and a rotation rate of 2500 rpm of the RDE. The numbers in the panels refer to the cycle number and "rev" denotes the respective reverse (anodic) scan. For clarity, the reverse scans of the other cycles are not shown. Steady-state measurements in 0.1 M CsOH were collected right after the eleventh CV.

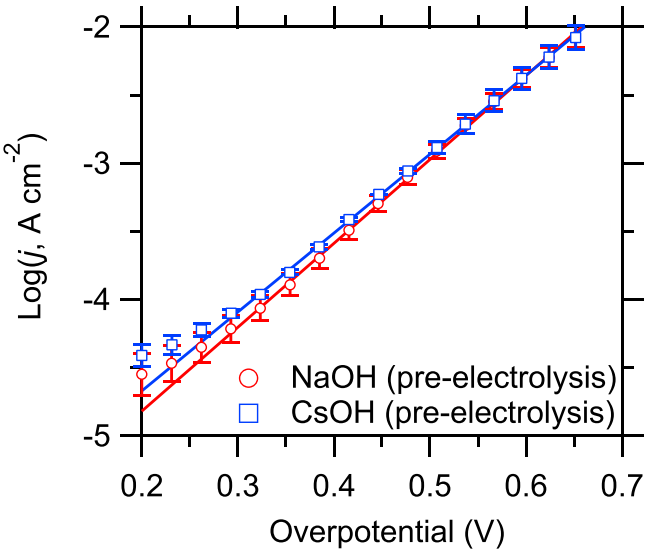

Figure 5. Tafel plots for the forward (cathodic) scans of the second CV in pre-electrolyzed electrolytes. The data represent the average of three independent experiments for each electrolyte. The error bars represent one standard deviation. For clarity, only a subset of the collected data points is shown on the plot. The Tafel plots for the 6th and 11th cycles are reported in Fig. S6.

ions is negligible at pH 13. As a result, alkali metal cations provide the counter charge in the electric double layer during cathodic polarization of the electrode. Fourth, low concentrations (10^{-2}–10^{-4} M) of Li^+ and Ba^{2+} were shown to enhance the HER on Ir/Ru alloy electrodes in 0.1 M KOH by up to nearly a factor of two.[23] Similar enhancements of the HER on Pt were found when switching from 0.1 M CsOH to LiOH electrolyte.[24] Therefore, the absence of a measurable cation effect on the HER is not necessarily expected.

As discussed in a recent review article,[19] there are numerous mechanisms by which cations can impact electrocatalytic processes. The predominant mechanism depends on the reaction conditions and electrode.[19] The prior observations of the dependence of the rate of the HER on cation identity are therefore not in contradiction of the results presented herein. Specifically, Danilovic et al. suggested that the hydrated cations are quasi-specifically adsorbed via surface-adsorbed hydroxide (OH_{ads}) on Ir/Ru alloys.[23] They hypothesized that these quasi-specifically adsorbed cations promote the HER by facilitating the dissociation of interfacial water. Such a mechanism is unlikely to be able to operate in the present case because the onset potential of the HER on Cu is about ≈300 mV more cathodic than on the Ir/Ru alloys. Under these cathodic potentials, the coverage of hydroxide on Cu is expected to be small.[33]

DFT models suggest that the specific adsorption of cations is possible under the experimental conditions employed in this work.[31,43] The absence of a measurable difference in the rate of the HER in Na^+- vs Cs^+-containing electrolyte suggests that the cation-specific electric fields are not significantly different from the perspective of the reacting water and/or that the surface-coverage of cations is not sufficiently large to impact the catalytic turnover.

DFT examination of the effects of cations on HER elementary processes.—To rationalize further our experimental findings, we used DFT calculations to examine possible impacts of alkali metal cations on HER elementary processes. For the computational model, we assumed a Cu(100) facet, which was previously identified as the predominant surface facet on polycrystalline Cu under electrochemical conditions.[37,44] The computational methods are described in the Supplementary Material. We first examined whether the presence of co-adsorbed alkali metal cations affects the strength of H binding to the surface through calculating the adsorption free energy of hydrogen (ΔG_H, calculated relative to half the gas phase free energy of H_2). The adsorption free energy of H has been used as a descriptor of HER catalyst performance.[45] The ΔG_H values of −0.07 eV for the bare Cu(100) surface at 1/9 monolayer is only slightly perturbed with Na^+ (−0.01 eV) or Cs^+ (−0.05 eV) co-adsorbed at the same coverage (Fig. S7). This minimal change in adsorption energy suggests the presence of alkali metal cations will have minor impact on H interaction with the Cu surface, and can be contrasted with a 0.25–0.4 eV change in CO binding energies to the Cu surface due to alkali cation co-adsorption.[46]

Cations could impact the HER rate by causing differences in the interfacial electric field, which has been reported to cause changes in the rates of elementary proton-coupled electron transfer steps involved in CO_2 reduction on Cu.[9,31] The Janik group has developed a simple approach to determine elementary electrochemical reaction barriers,[47] and applied this approach to approximate Volmer step barriers by examining water-assisted proton transfer steps on metal surfaces.[48] We examined whether variations in electric fields at the surface, due to changes in alkali metal cation, could cause significant changes in the Volmer barrier. We examined the impact of an externally applied field on the Volmer step. Initial, transition, and product state structures are shown in Fig. S8. As shown in Fig. S9, a cathodic potential would generate an electric field that causes a secondary, inhibitory effect on Volmer step kinetics. However, large variations in electric field would be necessary to cause a substantial effect on this barrier. An electric field difference of 0.3 V $Å^{-1}$ would be needed to produce a change in Volmer step barrier of ≈0.06 eV. Such a change in the activation barrier would cause a ten-fold change in the HER rate. We mapped the electric field resulting from Na^+ and Cs^+ cations adsorbed on the Cu(100) surface (Fig. S10). Electric fields of order 0.5 V $Å^{-1}$ or higher only occur within less than 1 Ångstrom from the cation, suggesting the Volmer step would need to occur at distances closer than the first hydration shell of the cations to experience electric fields sufficient to alter the HER kinetics. Though proving a negative result with DFT calculations is challenging given the multitude of mechanisms for cations to alter elementary processes, these DFT results corroborate the reported experimental results that alkali metal cations have insignificant impact on HER kinetics on Cu electrodes.

Conclusions

Herein, we investigated the effects of trace iron impurities and alkali metal cations on the HER on polycrystalline Cu electrodes in alkaline conditions. We found that iron impurities in commercially available hydroxide salts of the highest purity grades deposit on a Cu RDE over a timescale of tens of minutes. The deposition of iron leads to a substantial acceleration of the rate of the HER in 0.1 M CsOH (99.95%) by up to a factor of five over the course of eleven CVs. By contrast, at a lower pH of 9, the rate of iron deposition from an electrolyte of the same purity is markedly slower. The iron impurities can be effectively removed by pre-electrolyzing the solutions. In purified 0.1 M NaOH and CsOH, the HER current densities are almost identical, indicating the absence of a significant cation effect on the HER on Cu. In line with this experimental observation, our DFT model indicates that the surface binding energy of hydrogen, a descriptor of the HER, is only minimally perturbed by 1/9 of a monolayer of co-adsorbed cations. Further, the activation barrier of the Volmer elementary step of the HER is relatively insensitive to changes in the local electric field below ≈0.3 V $Å^{-1}$. Our findings show that Cs^+ can be employed to selectively promote desirable reaction, such as CO_2 reduction, in alkaline conditions. The thorough removal of trace iron impurities is essential for the effective suppression of the HER.

Acknowledgments

This work was supported by a CAREER award from the National Science Foundation (Award No.: CHE-1847841).

ORCID

Matthias M. Waegele https://orcid.org/0000-0002-1186-7545

References

1. K. P. Kuhl, E. R. Cave, D. N. Abram, and T. F. Jaramillo, "New insights into the electrochemical reduction of carbon dioxide on metallic copper surfaces." *Energy Environ. Sci.*, **5**, 7050 (2012).
2. Y. Hori, K. Kikuchi, A. Murata, and S. Suzuki, "Production of CO and CH_4 in electrochemical reduction of CO_2 at metal electrodes in aqueous hydrogencarbonate solution." *Chem. Lett.*, **14**, 1695 (1985).
3. M. Azuma, K. Hashimoto, M. Hiramoto, M. Watanabe, and T. Sakata, "Electrochemical reduction of carbon dioxide on various metal electrodes in low-temperature aqueous $KHCO_3$ media." *J. Electrochem. Soc.*, **137**, 1772 (1990).
4. K. P. Kuhl, T. Hatsukade, E. R. Cave, D. N. Abram, J. Kibsgaard, and T. F. Jaramillo, "Electrocatalytic conversion of carbon dioxide to methane and methanol on transition metal surfaces." *J. Am. Chem. Soc.*, **136**, 14107 (2014).
5. M. Duca, B. van der Klugt, and M. Koper, "Electrocatalytic reduction of nitrite on transition and coinage metals." *Electrochim. Acta.*, **68**, 32 (2012).
6. M. R. Singh, E. L. Clark, and A. T. Bell, "Effects of electrolyte, catalyst, and membrane composition and operating conditions on the performance of solar-driven electrochemical reduction of carbon dioxide." *Phys. Chem. Chem. Phys.*, **17**, 18924 (2015).
7. L. Sun, G. K. Ramesha, P. V. Kamat, and J. F. Brennecke, "Switching the reaction course of electrochemical CO_2 reduction with ionic liquids." *Langmuir*, **30**, 6302 (2014).
8. A. S. Varela, M. Kroschel, T. Reier, and P. Strasser, "Controlling the selectivity of CO_2 electroreduction on copper: the effect of the electrolyte concentration and the importance of the local pH." *Catal. Today*, **260**, 8 (2016).
9. J. Resasco, L. D. Chen, E. Clark, C. Tsai, C. Hahn, T. F. Jaramillo, K. Chan, and A. T. Bell, "Promoter effects of alkali metal cations on the electrochemical reduction of carbon dioxide." *J. Am. Chem. Soc.*, **139**, 11277 (2017).
10. J. O. Bockris and N. Pentland, "The mechanism of hydrogen evolution at copper cathodes in aqueous solutions." *Trans. Faraday Soc.*, **48**, 833 (1952).
11. N. Pentland, J. O. Bockris, and E. Sheldon, "Hydrogen evolution reaction on copper, gold, molybdenum, palladium, rhodium, and iron." *J. Electrochem. Soc.*, **104**, 182 (1957).
12. W. Sheng, M. Myint, J. G. Chen, and Y. Yan, "Correlating the hydrogen evolution reaction activity in alkaline electrolytes with the hydrogen binding energy on monometallic surfaces." *Energy Environ. Sci.*, **6**, 1509 (2013).
13. J. T. Feaster, A. L. Jongerius, X. Liu, M. Urushihara, S. A. Nitopi, C. Hahn, K. Chan, J. K. Nørskov, and T. F. Jaramillo, "Understanding the influence of [EMIM]Cl on the suppression of the hydrogen evolution reaction on transition metal electrodes." *Langmuir*, **33**, 9464 (2017).
14. P. Farinazzo Bergamo Dias Martins, P. Papa Lopes, E. A. Ticianelli, V. R. Stamenkovic, N. M. Markovic, and D. Strmcnik, "Hydrogen evolution reaction on copper: Promoting water dissociation by tuning the surface oxophilicity." *Electrochem. Commun.*, **100**, 30-33 (2019).
15. C.-T. Dinh et al., "CO_2 electroreduction to ethylene via hydroxide-mediated copper catalysis at an abrupt interface." *Science*, **360**, 783 (2018).
16. X. Chen, D. Henckel, U. Nwabara, Y. Li, A. I. Frenkel, T. T. Fister, P. J. A. Kenis, and A. A. Gewirth, "Controlling speciation during CO_2 reduction on cu-alloy electrodes." *ACS Catal.*, **10**, 672 (2020).
17. D. S. Ripatti, T. R. Veltman, and M. W. Kanan, "Carbon monoxide gas diffusion electrolysis that produces concentrated C_2 products with high single-pass conversion." *Joule*, **3**, 240 (2019).
18. K. J. P. Schouten, E. Pérez Gallent, and M. T. M. Koper, "The influence of pH on the reduction of CO and CO_2 to hydrocarbons on copper electrodes." *J. Electroanal. Chem.*, **716**, 53 (2014).
19. M. M. Waegele, C. M. Gunathunge, J. Li, and X. Li, "How cations affect the electric double layer and the rates and selectivity of electrocatalytic processes." *J. Chem. Phys.*, **151**, 160902 (2019).
20. C. M. Gunathunge, V. J. Ovalle, and M. M. Waegele, "Probing promoting effects of alkali cations on the reduction of CO at the aqueous electrolyte/copper interface." *Phys. Chem. Chem. Phys.*, **19**, 30166 (2017).
21. J. Li, X. Li, C. M. Gunathunge, and M. M. Waegele, "Hydrogen bonding steers the product selectivity of electrocatalytic CO reduction." *Proc. Natl. Acad. Sci. USA***116**, 9220 (2019).
22. P. Herasymenko and I. Šlendyk, "Wasserstoffüberspannung und adsorption der ionen." *Z. Phys. Chem. A*, **149**, 123 (1930).
23. N. Danilovic, R. Subbaraman, D. Strmcnik, A. P. Paulikas, D. Myers, V. R. Stamenkovic, and N. M. Markovic, "The effect of noncovalent interactions on the HOR, ORR, and HER on Ru, Ir, and $Ru_{0.50}Ir_{0.50}$ metal surfaces in alkaline environments." *Electrocatal.*, **3**, 221 (2012).
24. S. Xue, B. Garlyyev, S. Watzele, Y. Liang, J. Fichtner, M. D. Pohl, and A. S. Bandarenka, "Influence of alkali metal cations on the hydrogen evolution reaction activity of Pt, Ir, Au, and Ag electrodes in alkaline electrolytes." *ChemElectroChem*, **5**, 2326 (2018).
25. E. Liu, J. Li, L. Jiao, H. T. T. Doan, Z. Liu, Z. Zhao, Y. Huang, K. M. Abraham, S. Mukerjee, and Q. Jia, "Unifying the hydrogen evolution and oxidation reactions kinetics in base by identifying the catalytic roles of hydroxyl-water-cation adducts." *J. Am. Chem. Soc.*, **141**, 3232 (2019).
26. E. Pérez-Gallent, G. Marcandalli, M. C. Figueiredo, F. Calle-Vallejo, and M. T. M. Koper, "Structure- and potential-dependent cation effects on CO reduction at copper single-crystal electrodes." *J. Am. Chem. Soc.*, **139**, 16412 (2017).
27. L. Wang, A. Ambrosi, and M. Pumera, ""Metal-Free" catalytic oxygen reduction reaction on heteroatom-doped graphene is caused by trace metal impurities." *Angew. Chem. Int. Ed.*, **52**, 13818 (2013).
28. L. Trotochaud, S. L. Young, J. K. Ranney, and S. W. Boettcher, "Nickel-iron oxyhydroxide oxygen-evolution electrocatalysts: the role of intentional and incidental iron incorporation." *J. Am. Chem. Soc.*, **136**, 6744 (2014).
29. Y. Lum, Y. Kwon, P. Lobaccaro, L. Chen, E. L. Clark, A. T. Bell, and J. W. Ager, "Trace levels of copper in carbon materials show significant electrochemical CO_2 reduction activity." *ACS Catal.*, **6**, 202 (2016).
30. A. C. Garcia, T. Touzalin, C. Nieuwland, N. Perini, and M. T. M. Koper, "Enhancement of oxygen evolution activity of nickel oxyhydroxide by electrolyte alkali cations." *Angew. Chem. Inter. Ed.*, **58**, 12999 (2019).
31. S. A. Akhade, I. T. McCrum, and M. J. Janik, "The impact of specifically adsorbed ions on the copper-catalyzed electroreduction of CO_2." *J. Electrochem. Soc.*, **163**, F477 (2016).
32. K. Schouten, Y. Kwon, C. van der Ham, Z. Qin, and M. Koper, "A new mechanism for the selectivity to C_1 and C_2 species in the electrochemical reduction of carbon dioxide on copper electrodes." *Chem. Sci.*, **2**, 1902 (2011).
33. C. M. Gunathunge, V. J. Ovalle, Y. Li, M. J. Janik, and M. M. Waegele, "Existence of an electrochemically inert CO population on Cu electrodes in alkaline pH." *ACS Catal.*, **8**, 7507 (2018).
34. T. J. P. Hersbach, I. T. McCrum, D. Anastasiadou, R. Wever, F. Calle-Vallejo, and M. T. M. Koper, "Alkali metal cation effects in structuring Pt, Rh, and Au surfaces through cathodic corrosion." *ACS Appl. Mater. Inter.*, **10**, 39363 (2018).
35. D. Gao, I. Sinev, F. Scholten, R. M. Arán-Ais, N. J. Divins, K. Kvashnina, J. Timoshenko, and B. Roldan Cuenya, "Selective CO_2 electroreduction to ethylene and multicarbon alcohols via electrolyte-driven nanostructuring." *Angew. Chem. Inter. Ed.*, **58**, 17047 (2019).
36. H. Matsushima, C. Haak, A. Taranovskyy, Y. Gründer, and O. M. Magnussen, "In situ video STM studies of the hydrogen-induced reconstruction of Cu(100): potential and pH dependence." *Phys. Chem. Chem. Phys.*, **12**, 13992 (2010).
37. Y.-G. Kim, J. H. Baricuatro, A. Javier, J. M. Gregoire, and M. P. Soriaga, "The evolution of the polycrystalline copper surface, first to Cu(111) and then to Cu (100), at a fixed CO_2RR potential: a study by operando EC-STM." *Langmuir*, **30**, 15053 (2014).
38. E. Gileadi, *Physical Electrochemistry* (Wiley-VCH Verlag GmbH & KGaA, Weinheim, Germany) (2011).
39. A. J. Bard and L. R. Faulkner, *Electrochemical Methods: Fundamentals and Applications* (John Wiley & Sons, New York, NY) 2nd ed. (2000).
40. A. Holewinski and S. Linic, "Elementary mechanisms in electrocatalysis: revisiting the ORR Tafel slope." *J. Electrochem. Soc.*, **159**, H864 (2012).
41. D. Strmcnik, D. F. van der Vliet, K.-C. Chang, V. Komanicky, K. Kodama, H. You, V. R. Stamenkovic, and N. M. Marković, "Effects of Li^+, K^+, and Ba^{2+} cations on the ORR at model and high surface area Pt and Au surfaces in alkaline solutions." *J. Phys. Chem. Lett.*, **2**, 2733 (2011).
42. P. Atkins and J. de Paula, *Atkins' Physical Chemistry* (Oxford University Press, Oxford, United Kingdom) (2002).
43. J. N. Mills, I. T. McCrum, and M. J. Janik, "Alkali cation specific adsorption onto fcc(111) transition metal electrodes." *Phys. Chem. Chem. Phys.*, **16**, 13699 (2014).
44. K. Schouten, Z. Qin, E. Pérez Gallent, and M. T. M. Koper, "Two pathways for the formation of ethylene in CO reduction on single-crystal copper electrodes." *J. Am. Chem. Soc.*, **134**, 9864 (2012).
45. J. Greeley and J. K. Nørskov, "Large-scale, density functional theory-based screening of alloys for hydrogen evolution." *Surf. Sci.*, **601**, 1590 (2007).
46. D. Gao, I. T. McCrum, S. Deo, Y.-W. Choi, F. Scholten, W. Wan, J. G. Chen, M. J. Janik, and B. Roldan Cuenya, "Activity and selectivity control in CO_2 electroreduction to multicarbon products over CuO_x catalysts via electrolyte design." *ACS Catal.*, **8**, 10012 (2018).
47. G. Rostamikia, A. J. Mendoza, M. A. Hickner, and M. J. Janik, "First-principles based microkinetic modeling of borohydride oxidation on a Au(111) electrode." *J. Power Sources*, **196**, 9228 (2011).
48. S. Maheshwari, G. Rostamikia, and M. J. Janik, "Elementary kinetics of nitrogen electroreduction on Fe surfaces." *J. Chem. Phys.*, **150**, 041708 (2019).